GEOPHYSICAL RESEARCH LETTER, VOL. 20, NO. 8, PAGES 643-646, APRIL 23, 1993

MOMENT SPECTRA IN A SIMPLE MODEL OF AN EARTHQUAKE FAULT

Bruce E. Shaw
Institute for Theoretical Physics, University of California, Santa Barbara , CA 93106

Abstract The behavior of a simple one-dimensional, homogeneous, deterministic model of an earthquake fault is examined on the timescale of the rupture process. The model generates a complex spatial and temporal distribution of events from a frictional instability. I measure the frequency spectra of the moment release rate for events of different sizes, and observe power laws for the spectra. A bend in the spectra of large events is also observed. The paper concludes with a discussion of how these results may be relevant to real earthquake faults.

I. Introduction

An important goal in seismological research is the reconstruction of the earthquake source from seismographic signals. To obtain a set of source parameters, such as the location, seismic moment, and rupture length scale, measurements are averaged over a number of stations. The problem is made difficult by path effects as the signal, traveling through the inhomogeneous earth, is reflected and attenuated. A more fundamental problem confronts the seismologist seeking to reconstruct continuous fields defined on the rupture surface, such as the slip as a function of position on the fault: the set of one-dimensional time series measurements from seismograms contains less information than the two-dimensional source one would like to obtain. The problem is necessarily underdetermined. To obtain any kind of answer, therefore, one must assume certain constraints on possible source functions. Theoretical models of dynamic ruptures thus play a crucial role in guiding our assumptions. These models, or course, have their own built-in assumptions, and so it is useful to examine behavior of the simplest models. In this paper, I study the dynamics of a minimal earthquake model on the timescale of the rupture process. We have the advantage of complete knowledge of the entire history of each event, and of a complete catalogue which spans thousands of loading cycles. I take advantage of the large catalogue to measure the average moment spectra for events of different sizes; this is a measurement one would ideally like to make in the earth, but are hindered by errors due to path effects, and the limited number of events one can average over due to the long timescales– of order hundreds of years– of loading cycles. I observe a bend in the spectrum of large events which corresponds with the transition length scale from small to large events. I then use the privileged position of being able to view absolute displacements, and their time evolution in the model– something that cannot be done in the earth– to gain insight into the rupture process. It is seen that the large events are particularly simple; they involve one or two outgoing narrow pulses which travel down the fault at nearly constant speed, and roughly invert the displacement configuration.

The work presented in this paper is important for another reason. Previous work on self-organizing models [Bak, Tang, and Wiesenfeld, 1987] has focussed on complexity on longer timescales. The distribution of sizes of events [Carlson and Langer, 1989 (CL); Chen, Bak, and Obukhov, 1991; Nakanishi, 1990; Brown, Scholz, and Rundle, 1991], the time intervals between large events [Carlson, 1991], and the cycle of small event activity preceding large events [Shaw, Carlson, and Langer, 1992], have, among other things, been studied. In this paper I study model events on the timescale of the rupture process itself. Understanding the source on this timescale is important, both because of potential applications to hazard estimates of what kind of shaking may occur, and because of the possibility of comparing with the wealth of information available from seismograms.

Paper number 92GL02437
0094-8534/93/92GL-02437$03.00

The paper is organized as follows. Section II introduces the model. Section III presents the new work from numerical simulations of the model. Measurements of the average moment spectra, the time history of an individual event, and the roughness of the displacement field are shown. The paper concludes in section IV by discussing how these results may apply to real earthquakes.

II. The Model

The simplest differential equation with the minimal ingredients of elastic coupling, a loading mechanism, and a frictional instability is given by [CL]

$$\ddot{U} = U'' - U - \phi(\dot{U} + \nu) \tag{1}$$

U is the displacement field. Dots denote differentiation with respect to dimensionless time t, while primes denote differentiation with respect to space s. Time has been scaled by the slip time of a uniformly slipping fault. Distance has been scaled so that the speed of sound is unity. The plate loading rate is ν, which is a very small number. All the nonlinearity is in the friction function ϕ, which depends only on the velocity. It is a stick-slip velocity-weakening function. Equation (1) says that the acceleration of the displacement field is the sum of three forces acting on it: a compressional stress, a shear stress, and friction.

The form of the friction function ϕ used in this paper is shown in Figure 1, and is given by

$$\phi(z) = \phi_0 + \begin{cases} (-\infty, 1), & z = 0, \\ \frac{1-\sigma}{1+2\alpha z/(1-\sigma)}, & z > 0 \end{cases} . \tag{2}$$

The difference between the maximum sticking friction and the minimum sliding friction sets the scale of the change in U during an event. This is set to unity. The minimum sliding friction ϕ_0 sets the zero of U; note that there is a symmetry in the equation of motion (1), that $\phi \to \phi + constant$ and $U \to U - constant$ leaves the equations unchanged. If ϕ_0 is large enough compared to unity, the fault will never overshoot, and backward motion will not occur. This is the situation considered in Eq. (2), and is represented by the sticking friction being unbounded from below. The constant ϕ_0 plays no role

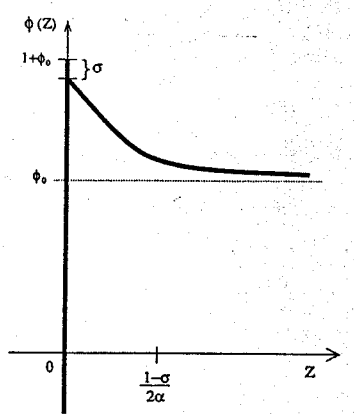

Fig. 1. The velocity-weakening slip-stick friction force $\phi(z)$, given in Eq. (2). The friction ϕ depends only on the velocity z. When sticking, the friction $\phi(0)$ satisfies $\phi(0) \lesssim \phi_0 + 1$, while slipping friction drops to an initial value of $\phi(0^+) = \phi_0 + 1 - \sigma$ and then gets smaller with increasing velocity. Note that the equations of motion (1) and (3) are invariant with respect to adding a constant to the friction ϕ, and subtracting that same constant from the displacement U. Without loss of generality, then, ϕ_0 can be set to zero.

in the dynamics, and can be set to zero without loss of generality. The parameters α and σ which represent how the friction changes, and are described below, are thus the only relevant parameters in (2). Physically, what all this means is that stress drops are set by the difference between sticking and sliding friction, and the absolute stress, set by ϕ_0, does not affect anything. The ratio of the minimum sliding friction to the maximum sticking friction, $\phi_0/(\phi_0+1)$, can thus be an arbitrarily large fraction, depending on how big ϕ_0 is, and the model gives the same results.

Friction keeps the field stuck, with $z = 0$, until its maximum value $\phi_0 + 1$ is exceeded. During the sticking phase, the multivalued friction exactly balances the other two forces, and the fault is uniformly loaded with $\dot{U} = -\nu$. Once the threshold is exceeded, slipping occurs. Slipping events start with acceleration σ, which sets the scale of the smallest events [Carlson, Langer, Shaw, and Tang, 1991 (CLST)]. The parameter α represents the amount of velocity weakening; this is the crucial instability in the problem, and a linear stability analysis shows all Fourier modes grow exponentially while slipping in the velocity weakening regime $d\phi(z)/dz < 0$ [CL]. There is one other important parameter, the smallest lengthscale $1/\ell$. The nonlinearities in the friction develop shock-like waves which depend on a cutoff lengthscale in the problem [Langer and Tang, 1991]. This smallest lengthscale shows up in the statistics of even the largest events [CLST].

The simplest spatial discretization of this partial differential equation gives the classic block and spring model in seismology of Burridge and Knopoff [1967], shown in Figure 2. The coupled ordinary differential equations for this system are

$$\ddot{U}_j = \ell^2(U_{j+1} - 2U_j + U_{j-1}) - U_j - \phi(\dot{U}_j + \nu) \quad . \tag{3}$$

The smallest lengthscale $1/\ell$ is now the average spacing of the blocks a. This is the model I study numerically in this paper.

An event occurs when a block reaches the threshold for slipping. It may or may not cause its neighbors to slide. The size of the event, the 'moment', is then the sum of the change in the displacements of all the blocks that moved:

$$M = \sum_j \delta U_j, \tag{4}$$

The magnitude of an event is the logarithm of this moment. Beginning from any nonsmooth initial condition, the system reaches a statistically steady state where a 'noisy' sequence of events is observed, with a distribution of sizes of events which is consistent with what is seen for single faults. A typical distribution of sizes of events for small σ and $\alpha > 1$ is shown in Figure 3. Two different types of events, small and large, are seen. The small events satisfy the Gutenberg-Richter law [1954], showing a power law distribution of rate R of events with moments between M and $M + \delta M$ of the form $R(M) \sim M^{-(1+b)}$, where b is the "b-value" of the distribution. The large events occur at a rate in excess of what would be expected from extrapolating the small event scaling rate [CL]. This is also seen along certain major faults where sufficient data is available [Wesnousky, Scholz, Shimazaki, and Matsuda (1983); Singh, Rodriguez, and Esteva (1983); Schwartz and Coppersmith (1984); Davison and Scholz (1985)]. In this paper, we examine the parameter regime σ small and $\alpha > 1$ since there, the small events show a

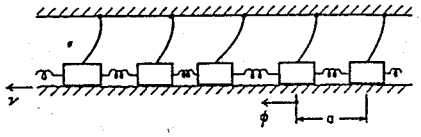

Fig. 2. The block and spring model, given in Eq. (3), consists of a one dimensional chain of equal masses. Each block is joined to its nearest neighbors by coupling springs of equal strength. Pulling springs of equal strength attach the blocks to a fixed plate. They are in contact with another plate which is moving at constant velocity ν. Between each block and the moving plate there is a friction force ϕ which depends only on the velocity of the block. The equilibrium spacing between the blocks is a.

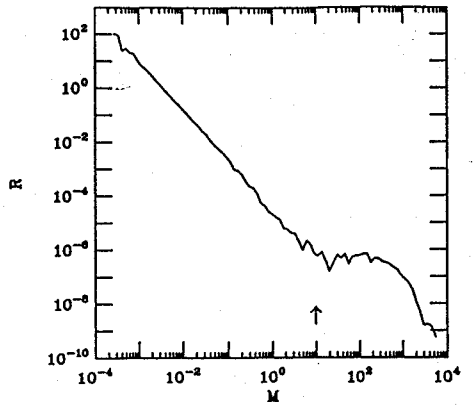

Fig. 3. The distribution of sizes of events. The vertical axis is rate of events having moments between M and $M + \delta M$, and the horizontal axis moment M . The arrow in this figure marks the calculated transition moment $\widetilde{M}$, given by Eq. (5). The parameters in the model used for this figure are $\ell = 10$, $\alpha = 2$, and $\sigma = .01$.

generic b-value exponent of 1. For smaller α, the exponent changes continuously with α.

The transition between large and small events can be calculated approximately, and is discussed in references [CL] and [CLST]. Here, I simply quote the results. The transition moment $\widetilde{M}$ is

$$\widetilde{M} = \frac{2}{\alpha} \tag{5}$$

and the corresponding lengthscale $\widetilde{\xi}$ where the transition between small and large events occurs is

$$\widetilde{\xi} = \frac{2}{\alpha}\ln(\frac{4\ell^2}{\sigma}). \tag{6}$$

In addition to the distribution of sizes of events, a number of other properties have been observed to change between small and large events in the model [CLST]. In what follows, further differences will be seen.

III. Numerical Results

The work in this paper concerns the dynamics of events on the timescale of the rupture process. We look at the coherent motion of the blocks, studying the time evolution of the moment rate

$$\dot{M}(t) = \sum_j \dot{U}_j(t). \tag{7}$$

The moment spectrum of an individual event is obtained by Fourier transforming the moment rate:

$$\hat{M}(\omega) = \int \dot{M}(t)e^{i\omega t}dt. \tag{8}$$

These events are divided into groups of similar sizes, and then the absolute value of the amplitudes $\hat{M}(\omega)$ are averaged. Figure 4 shows average moment spectra. The 7 different curves are for groups of events of different sizes; the zero frequency moment $\hat{M}(0)$ corresponds with the moment plotted in Figure 3. The two different types of events, large and small, show different spectra. For the large events, the top 3 curves in Figure 4, we numerically observe three power law regions:

$$\hat{M}(\omega) \sim \begin{cases} \omega^0, & \omega \lesssim \frac{2\pi}{M} \\ \omega^{-1}, & \frac{2\pi}{M} \lesssim \omega < \frac{2\pi}{\xi} \\ \omega^{-\gamma}, & \frac{2\pi}{\xi} < \omega \end{cases} \qquad M > \widetilde{M} \, . \tag{9}$$

When σ is small and $\alpha \gtrsim 1$, the exponent γ has been observed numerically to have the value $\gamma = 5/2$. The reason this value occurs is not clear. An explanation of the other two exponents will be given shortly. The first bend, where the amplitude changes from ω^0 to ω^{-1}, occurs at the "corner frequency", given roughly by the sound speed divided by the rupture length Δ. The second bend, where

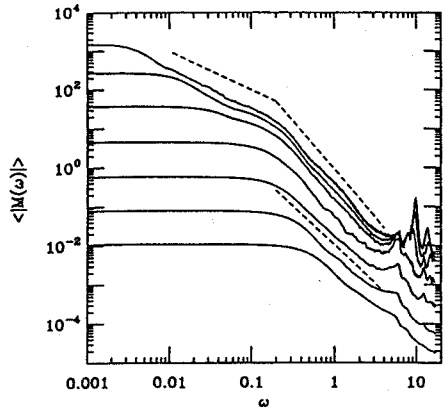

Fig. 4. The average moment spectra $\langle|\hat{M}(\omega)|\rangle$ versus $\omega/2\pi$ is plotted on a log-log scale, showing 7 different size groups. The zero frequency moment $\hat{M}(0)$ corresponds to the moments M in figure 3. The parameters used for this figure are $\ell = 10$, $\alpha = 2$, and $\sigma = .01$. For these parameters, the calculated transition frequency between small and large events is $\tilde{\omega}/2\pi = .095$, somewhat underestimating where the bend in the large events spectra occurs. Dashed lines with slope -1 bending to $-5/2$, and with slope -2 are drawn on the figure.

the amplitude begins to drop off as $\omega^{-\gamma}$, occurs at the frequency $\tilde{\omega} = 2\pi/\tilde{\xi}$, where $\tilde{\xi}$ is the length scale marking the transition between large and small events.

Looking towards the highest frequencies, we see a peak in the spectrum. This peak corresponds to the sound speed divided by the smallest lengthscale a , the block size, and occurs at $\omega_0/2\pi = \ell$. A smaller peak at the two block frequency can also be seen.

A different scaling is observed for the small events, the 4 bottom curves in Figure 4:

$$\hat{M}(\omega) \sim \begin{cases} \omega^0, & \omega \lesssim \frac{2\pi}{\Delta} \\ \omega^{-2}, & \frac{2\pi}{\Delta} \lesssim \omega \end{cases} \qquad M < \widetilde{M}. \qquad (10)$$

For the small events, the amplitudes of the high frequencies falls as ω^{-2} . Also, there is only one bend in the curve, at the corner frequency, which is related to the rupture length. When σ is large, the corner frequency is just the rupture length divided by the sound speed, as in the large events. When σ is small, however, the rupture typically remains open across the width of the rupture zone, and, by closing back up from the edge of the rupture, can last up to twice as long. This effect, of a relatively longer event duration for small σ, was noted in [CLST].

Let's examine the rupture process by following the displacements in time. Figure 5 illustrates a typical large event. Away from the epicenter, large events consist of one or two narrow pulses traveling out from the epicenter at approximately the sound speed. Only a small portion of the fault is slipping at any given time. This behavior is not seen in the classic fault-slip models [e.g. Kostrov, 1964, and Madariaga, 1976] but is similar to what is seen in the model of Heaton [1990]. Each pulse basically inverts the U field; potions of the fault that were initially farther back move more, while parts that were less far back move less. (Recall that the constant value of the friction ϕ_0 was subtracted from U in the normalization, and that really there is no overshoot, in the sense that the shear stress is always pointing in the same direction).

Figure 5 also shows large fluctuations in the moment release rate; the variations in the rate are of order the rate itself. This produces a signal with "subevents", as they are known in the seismological literature.

Another thing that can be seen in Figure 5 is that the rupture velocity varies as the pulse travels over regions that are more and less stuck. Langer and Tang [1991] have calculated analytically the velocities in the case of pulses traveling into uniformly stuck regions. While variations in the rupture velocity can be seen, the variations are only a small fraction of the average rupture velocity, and variations in the moment rate are dominated by variations in the particle velocities. A plot of final slip and maximum particle velocity along the fault show the two quantities to be roughly proportional to each other.

The fluctuations in the moment rate are caused by the roughness of the U field. How are they related? To quantify the roughness of the U field, we measure the spatial Fourier transform of U, averaging the absolute value of the amplitudes over a number of different configurations. Figure 6 is a plot of the transform $\hat{U}(k)$, where k is the wavenumber. For $k > 2\pi/\tilde{\xi}$, $\hat{U}(k) \sim k^{-2}$. This scaling corresponds to discontinuous changes in the derivative of U along the fault. The ω^{-2} high frequency falloff of the small events is a result of the discontinuous velocities the small pulses respond with as they pass over the discontinuous stresses on the model fault. For the large events, having the high frequency falloff being faster than ω^{-2} means the large pulses are responding more continuously, in a more averaged way. Turning towards length scales larger than $\tilde{\xi}$, for $2\pi/\xi^* < k < 2\pi/\tilde{\xi}$, where ξ^* is the length of the largest events, we have $\hat{U}(k)$ scales as k^{-1} only roughly– less well than $\hat{M}(w)$ seems to scale in that range. The origin of the ω^{-1} intermediate region of the large events is therefore probably due to the finite duration, and steep rise of $\dot{M}(t)$; approximating the moment release rate by a square pulse in $\dot{M}(t)$ gives an ω^{-1} scaling for frequencies above the corner frequency.

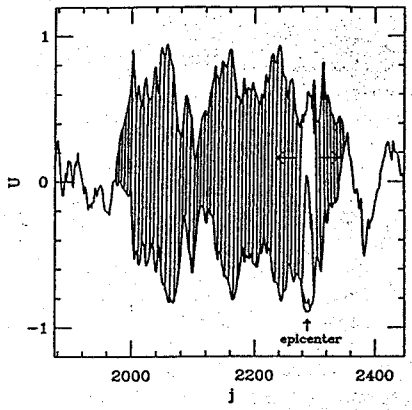

Fig. 5. A large event rupture. I have superposed a series of snapshots taken at equally spaced times during the rupture, showing the displacement U of the blocks as a function of position j in each snapshot. The steeply inclined lines are the blocks that are moving between the initial configuration below and the final configuration above. The epicenter is marked with an arrow. There are two outgoing narrow pulses emanating from the epicenter. The two opposite pointing arrows emphasize the directions of the outgoing pulses. The parameters used in the figure are $\ell = 3$, $\alpha = 1.2$, and $\sigma = .01$.

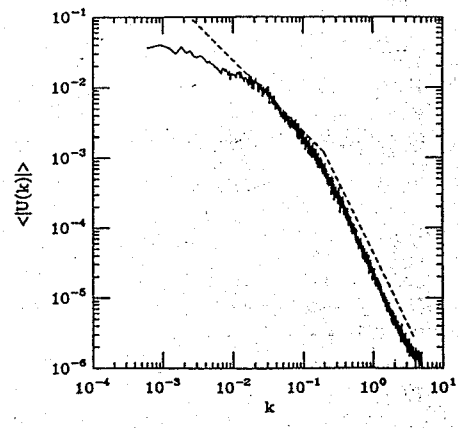

Fig. 6. The average spatial Fourier spectra of the displacement field U. The vertical axis is $\langle|\hat{U}(k)|\rangle$ and the horizontal axis is k. The dashed line has slope -1 bending to -2 (the bend is put at .2, which appears to fit the data better than the calculated transition of .095). The parameters used for this figure are $\ell = 10$, $\alpha = 2$, and $\sigma = .01$

IV. Conclusion

How do the results for the model compare with the real Earth, and what questions are posed by this work? The first result to compare is the moment spectra. At the most basic level, power laws are seen in both the model and in the Earth. At the next level, we want to compare the values of the exponents. For the small events in the model, the high frequency falloff is ω^{-2}. While seismological measurements of the exponent of the high frequency falloff depend on assumptions about the frequency dependence of attenuation, a falloff of ω^{-2} is most often what is reported to be observed [see, e.g., Hanks and McGuire, 1981]. It is interesting to note that in the model, the high frequency falloff for large events is actually slightly steeper than ω^{-2} . While the reason this occurs in the model is not entirely clear, it would be very interesting if this were also true in the earth. One way to test this might be to compare the falloff of small events with the falloff of large events, to see if the falloff of large events might be systematically steeper.

A second result from the model that seems likely to hold in the Earth, is the inversion of the displacement field during large events; places that were initially farther back move more, while places that were less far back move less. One consequence of this that might be observable is that for faults where there is no aseismic creep, places that moved far in the last large event would be the places that would tend to move less in the next large event, and vice versa. The problems with observing this in practice is the long repeat time between large events, and the need for a nearby array of instruments to do accurate reconstruction of slip along the fault.

A third result is the bend in the spectra of large events that occurs at the lengthscale corresponding to the transition between small and large events in the model. At this lengthscale, many properties have been seen to change, including the distribution of sizes of events. Might there also be a similar bend in the spectra of large events in the Earth at a lenghtscale corresponding to a change in the distribution of sizes of events? Recent measurements have suggested that there may be a change in the distribution of sizes of events occurring at the lengthscale corresponding to the brittle crust width (15 kilometers on strike-slip faults, and around 50 kilometers on subduction zones) [Pacheco, Scholz, and Sykes, 1992]. Boatwright and Choy [1989] have reported observations that suggest there may be a bend in the spectrum at these brittle crust lengthscales, though it is currently an open question [for other data, see Hartzel and Heaton, 1985; Houston and Kanamori, 1986]. Bends are particularly important to look for observationally, as they are robust features which do not depend on smooth corrections due to attenuation.

Finally, this work has examined motions in the far-field. By including retardation effects, the model can also generate near field motions. One great advantage of this model is that source motions and rupture velocities do not have to be assumed, but rather arise from the dynamical equations. Success in producing a realistic synthetic radiation source could have a number of applications, in fields such as inversion seismology and earthquake engineering.

Acknowledgements. Jim Langer provided many helpful comments in preparing this manuscript. I have also benefited from discussions with Jean Carlson, Craig Nicholson, and Chao Tang. Supported by NSF Grant No. PHY89-04035, the U.S. Department of Energy Grant DE-FG03-84ER45108, and the Southern California Earthquake Center .

References

Bak, P., C. Tang, and K. Wiesenfeld, Self-Organized Criticality: An Explanation of $1/f$ Noise, *Phys. Rev. Lett., 59*, 381, 1987.

Boatwright, J., and G.L. Choy, Acceleration Spectra for Subduction Zone Earthquakes, *J. Geo. Res., 94*, 15541-54, 1989.

Brown, S.R., C.H. Scholz, and J.B. Rundle, A Simplified Spring Block Model of Earthquakes, *Geophys. Res. Let., 18*, 215, 1991.

Burridge, R., and L. Knopoff, Model and Theoretical Seismicity, *Bull. Seis. Soc. Am., 57*, 341, 1967.

Carlson, J.M., and J.S. Langer, Mechanical Model of an Earthquake Fault, *Phys. Rev. A 40*, 6470, 1989.

Carlson, J.M., Time Intervals Between Large Earthquakes and Correlations With Smaller Events: An Analysis Based on a Mechanical Model of a Fault, *J. Geo. Res., 96* , 4255, 1991.

Carlson, J.M., J.S. Langer, B.E. Shaw, and C. Tang, Intrinsic Properties of a Burridge-Knopoff Model of an Earthquake Fault, *Phys. Rev. A, 44*, 884, 1991.

Chen, K., P. Bak, and S.P. Obukhov, Self Organized Criticality in a Crack-Propagation Model of Earthquakes, *Phys. Rev. A, 43*, 625, 1991.

Davison, F.C., and C.H. Scholz, Frequency-Moment Distribution of Earthquakes in the Aleutian Arc: A test of the Characteristic Earthquake Model, *Bull. Seis. Soc. Am. 75*, 1349, 1985.

Gutenberg, B., and C.F. Richter, Seismicity of the Earth and Related Phenomena, Princeton University Press, Princeton, NJ, 1954.

Hanks, T.C., and R.K. McGuire, The Character of High-Frequency Strong Ground Motion, *Bull. Seis. Soc. Am., 71*, 2071, 1981.

Hartzel, S.H. and T.H. Heaton, Teleseismic Time Functions for Large Subduction Zone Earthquakes, *Bull. Seis. Soc. Am, 75*, 965-1004, 1985.

Heaton, T., Evidence for and Implications of Self-Healing Pulses of Slip in Earthquake Rupture, *Phys. Earth and Plan. Int. , 64*, 1-20, 1990.

Houston, H., and H. Kanamori, Source Spectra of Great Earthquakes: Teleseismic Constraints on Rupture Process and Strong Motion , *Bull. Seis. Soc. Am., 76*, 19-42, 1986.

Kostrov, B.V., Self Similar Problems of Propoagation of Shear Cracks, *J. Appl. Math. Mech., 28*, 1077-87, 1964.

Langer, J.S., and C. Tang, Rupture Propagation in a Model of an Earthquake Fault, *Phys. Rev. Lett., 67*, 1043, 1991.

Madariaga, R., Dynamics of an Expanding Circular Fault, *Bull. Seis. Soc. Am., 66*, 636-66, 1976.

Nakanishi, H., Cellular-automaton Model of Earthquakes with Deterministic Dynamics, *Phys. Rev. A, 41*, 7086, 1990.

Pacheco, J.F., C.H. Scholz, and L.R. Sykes, Changes in Frequency Size Relationship From Small to Large Earthquakes, *Nature, 355*, 71-3, 1992.

Schwartz, D.P., and K.J. Coppersmith, Fault Behavior and Characteristic Earthquakes: Examples From the Wasatch and San Andreas Fault Zones, *J. Geo. Res. 89*, 5681, 1984.

Shaw, B.E., J.M. Carlson, and J.S. Langer, Patterns of Seismic Activity Preceding Large Earthquakes, *J. Geo. Res., 97*, 479-88, 1992.

Singh, S., M. Rodriguez, and L. Esteva, Statistics of Small Earthquakes and Frequency of Occurrence of Large Earthquakes Along the Mexican Subduction Zone, *Bull. Seis. Soc. Am., 73*, 1779-96, 1983.

Wesnousky, S.G., C.H. Scholz, K. Shimazaki and T. Matsuda, Earthquakes Frequency Distribution and the Mechanics of Faulting, *J. Geo. Res.88*, 9331, 1983.

Shaw, B. Institute for Theoretical Physics, University of California, Santa Barbara, CA 93106-4030.

(Received: April 16, 1992;
Revised: October 9, 1992;
Accepted: October 12, 1992.)